LAWRENCE
LIVERMORE
NATIONAL
LABORATORY

LLNL-JRNL-670642

The High Pressure Structure and Equation of State of 2,6-diamino-3,5-dinitropyrazine-1-oxide (LLM-105) up to 20 GPa: An Experimental and First Principles Simulations Investigation

E. Stavou, R. M. Manaa, J. M. Zaug, I. W. Kuo, P. F. Pagoria, J. C. Crowhurst, M. R. Armstrong, B. Kalkan

May 13, 2015

Journal of Chemical Physics

Disclaimer

The High Pressure Structure and Equation of State of 2,6-diamino-3,5-dinitropyrazine-1-oxide (LLM-105) up to 20 GPa: An Experimental and First Principles Simulations Investigation

Elissaios Stavrou,[1, a)] M. Riad Manaa,[1, b)] Joseph M. Zaug,[1] I-Feng W. Kuo,[1] Philip F. Pagoria,[1] Bora Kalkan,[2, 3] Jonathan C. Crowhurst,[1] and Michael R. Armstrong[1]

[1)] *Lawrence Livermore National Laboratory, Physical and Life Sciences Directorate, P.O. Box 808 L-350*

[2)] *Advanced Light Source, Lawrence Berkeley Laboratory, Berkeley, California 94720, United States*

[3)] *Advanced Materials Research Laboratory, Department of Physics Engineering, Hacettepe University 06800, Beytepe, Ankara, Turkey*

(Dated: 12 May 2015)

Recent theoretical studies of 2,6-diamino-3,5-dinitropyrazine-1-oxide ($C_4H_4N_6O_5$ Lawrence Livermore Molecule No.105, LLM-105) report unreacted high pressure equations of state that include several structural phase transitions while one published experimental study reports EOS data up to a pressure of 6 GPa with no observed transition. Here we report the results of a synchrotron-based X-ray diffraction study and also ambient temperature isobaric-isothermal atomistic molecular dynamics simulations of LLM-105 up to 20 GPa. We find that the ambient pressure phase remains stable up to 20 GPa; there is no indication of a pressure induced phase transition. We do find a prominent decrease in *b*-axis compressibility starting at approximately 13 GPa and attribute the stiffening to a critical length where inter-sheet distance becomes similar to the intermolecular distance within individual sheats. The ambient temperature isothermal equation of state was determined through refinements of measured X-ray diffraction patterns. The pressure-volume data was fit using various EOS models to yield bulk moduli with corresponding pressure derivatives. We find very good agreement between the experimental and theoretically derived EOS.

[a)]E-mail E.S. stavrou1@llnl.gov

[b)]E-mail M.R.M. manaa1@llnl.gov

I. INTRODUCTION

Low thermal and shock sensitivity and high energy density are among the most important characteristics of a useful energetic high explosive material. 2,6-diamino-3,5-dinitropyrazine-1-oxide ($C_4H_4N_6O_5$ Lawrence Livermore Molecule No.105, LLM-105) stands out as a very promising candidate due to its low insult sensitivity and high energy output. Indeed, experimental studies reveal that LLM-105 (usually in the form of a plastic ponded-polymeric matrix formulation e.g. with Kel F-800[1]) sensitivity is between the 1, 3, 5-triamino-2, 4,6-trinitrobenzene (TATB) a highly insensitive explosive, and octahydro-1, 3, 5, 7-tetranitro-1, 3, 5, 7-tetrazine (HMX), which is more sensitive.[2] Additionally, the energetic content of LLM-105 is also between TATB and HMX (about 20% above TATB and 15 % below HMX).[3] LLM-105 was first synthesized in 1998[4] and it has attracted considerable experimental[5–10] and theoretical[11–14] interest for the aforementioned reasons. From these studies, a detonation velocity >7500 m/s (depending on the formulation[9,15]) and a detonation pressure >30 GPa have been reported. Moreover, LLM-105 remains stable up to $\approx$ 530 K, where decomposition occurs at ambient pressure.[8] Engineering design initiatives have also been focused to produce energetic micro- and nano-structured devices; and recently, one such project yielded LLM-105 microtubes.[6]

LLM-105 crystalizes in a monoclinic structure (SG: $P2_1/n$ (14), Fig. 1) with four formula units per unit cell[5] and its relatively high stability should arise from the existence of intra-[12] and inter-[16] molecular hydrogen H$\cdots$ O bonds. The high pressure structural behavior of LLM-105 has been studied both theoretically[13,14] (T= 0 K) up to $\approx$ 50 GPa and experimentally[8] up to 5.5 GPa. A series of structural phase transitions at 8, 17, 25 and 42 GPa have been proposed by Wu *et al.*[14] based on irregular changes of lattice parameters. More recently, Manaa *et al.*[13] concluded that the ambient pressure phase of LLM-105 remains stable up to 45 GPa. Both theoretical studies suggest that LLM-105 exhibits highly anisotropic compressibility, *i.e.* a and c axes are much stiffer than the b-axis. Because experimental results of LLM-105 were reported only up to a maximum 5.5 GPa, the issue of structural behavior at higher pressures must be re-examined and established. Moreover, an accurate determination of the room-temperature high-pressure unreacted EOS is essential for continuum based simulations of physical and mechanical properties and performance under loading conditions..[13]

In this work, we have conducted a detailed X-ray diffraction (XRD) and first principles room temperature computational simulations of LLM-105 up to 20 GPa. We implemented dispresion-corrected density-functional theory (DFT) based isothermal-isobaric molecular dynamics simulations (T= 300 K) at various pressures for single crystal LLM-105. We find from both the experimental and computational results that LLM-105 remains in the ambient phase up to the highest pressure of this study without any sign of a structural phase transition. The simulation results are found to be in very good agreement with the experimentally determined EOS up to 20 GPa. It is established that LLM-105 clearly exhibits anisotropic compression; up to 13 GPa, compressibility along the b-axis is measurably higher than along the a and c axes.

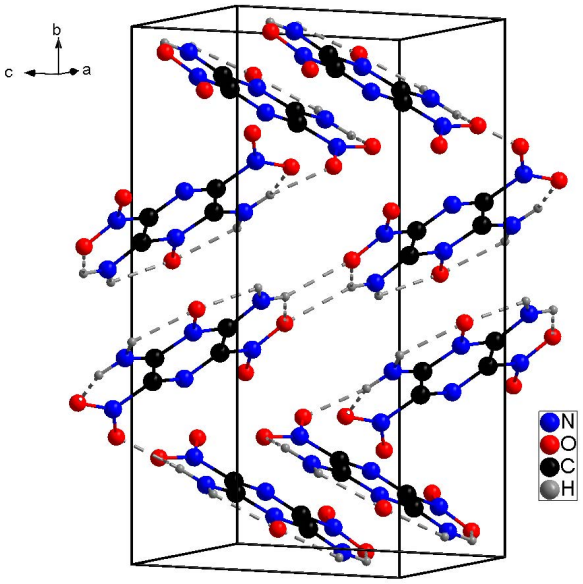

FIG. 1. Schematic representation of the ambient pressure monoclinic LLM-105 phase. Intra-[12] and inter-[16] hydrogen bonds are indicated with dashed grey lines.

II. METHODS

A. Experimental

LLM-105 was synthesized with a 57% yield by the nitration of 2,6-diaminopyrazine-1-oxide (DAPO) with a mixture of 100% HNO_3 and 10% fuming sulfuric acid at 20-30 ^{o}C for 3h. Recrystallization was achieved by dissolving LLM-105 as a 2.5% solution in N,N-

dimethylformamide (DMF) at 120 ^{o}C, and by slowly adding two volumes of warm water and allowing the mixture to cool to $\sim$ 40 ^{o}C. The LLM-105 crystal habit typically exhibits as brilliant yellow rods. Additional details of the synthesis procedure can be found in Ref. [4].

LLM-105 single crystals where ground to a fine powder for x-ray diffraction measurements. The sample including pressure sensors were loaded into diamond-anvil cell (DAC) sample chambers. For each of two x-ray studies, rhenium gaskets (preindented to 40-45 μm thick using 400 μm culets) were used to radially confine the pressurized samples. Initial sample chamber diameters were nominally 150 μm. Silicone oil was utilized as a pressure-transmitting medium (PTM): it is relatively inert, easy to load, and does not exhibit Bragg diffraction peaks. A MAR355 CCD detector was used to collect pressure dependence X-ray diffraction data at the Advanced Light Source Beamline 12.2.2 (x-ray spot size is $\sim$10μmx10μm and λ=0.4959Å). To minimize the possibility of x-ray induced decomposition, diffraction measurements were never repeated at the same spatial position within the sample. Pressure was determined using a known ambient temperature EOS of gold[17] and also calibrated ruby luminescence.[18] The maximum pressure uncertainty was less than 0.2 GPa at the highest pressure achieved in this study where also the deviatoric stress within the PTM exceeds 3 GPa.[19] Powder diffraction patterns were integrated using the FIT2D2[20] program to yield scattering intensity versus 2θ diagrams.

B. Computational methods

The reported calculations were performed using the description of our previous study, which determined the cold compression curve (T= 0 K) of LLM-105, among other properties.[13] Briefly, we use DFT within the generalized gradient corrected approximation of PerdewBurkeErnzerhof (PBE) for the exchange-correlation potential.[21] Lack of dispersion interaction in DFT was corrected for with the inclusion of two-body (D2) dispersion correction as proposed by Grimme.[22] A dual basis set formalism for the description of wavefunctions and for electron density was utilized. A triple zeta with double polarization (TZV2P) Gaussian type orbital basis was implemented for the wavefunctions, while plane wave basis expanded to 320 Ry is used to represent the electron density. The core electronic states are represented by the norm conserving Goedecker-Teter-Hutter pseudopotentials.[23] For cell/geometry optimization, the following convergence criteria were implemented: total en-

ergy was converged to a tolerance of less than 1×10^{-5} eV/atom, the residual forces to less than of 0.03 eV/Å, the residual stress to less than 0.05 GPa, maximum displacement to less than 0.001 Å, and the self-consistent field convergence criterion of 5×10^{-7} eV/atom. The isobaric-isothermal molecular dynamics simulation is carried out following the recipe outlined by Schmidt *et al.*[24] The wavefunctions are explicitly minimized to 10^{-7} Hartree using the orbital transformation method for every dynamics step.[25] Forces are then utilized to propagate the molecular dynamics simulation in the isothermal-isobaric ensemble (NPT) with a fixed time step of 0.5 fs. Simulations were conducted at T= 300 K, with temperature being controlled via individual Nos-Hoover chains coupled to each degree of freedom with a coupling constant of 2000 cm^{-1}.[26,27] The barostat characteristic frequency was set to 500 fs. The calculations were performed on a supercell of dimension 3×1×2 (containing 24 LLM-105 molecules, 456 atoms) using the Quickstep module within the CP2K simulation suite.[28,29]

III. RESULTS

In Figure 2(a), the experimental ambient pressure xrd pattern of LLM-105 is presented together with the calculated pattern according to Ref. [5]. A perfect agreement between these two patterns can be observed thus indicating the absence of solid impurities in the starting LLM-105 specimen. Slight differences of relative intensity are normally attributed to preferred orientation effects in the powder pattern. In Figure 3, selected pressure dependent x-ray powder diffraction patterns of LLM-105 are presented. All except one of the observed peaks in this pressure range can be indexed with the ambient phase monoclinic structure. The intense additional Bragg peak, indicated with red arrows in Figure 3, appears as a complete diffraction ring in 2D XRD images at very low pressures e.g., 0.1 GPa. It shifts to higher angles (lower d-spacing) with increased pressure and gradually decreases in relative intensity up to approximately 19 GPa where it virtually disappears. While the very "clean"ambient pressure LLM-105 diffraction pattern (Fig. 2(a)) rules out the presence of a solid impurity, pressure-induced crystallization of a liquid impurity would result in more than one Bragg peak. The same peak has been also observed in a previous independent XRD study of LLM-105 under pressure.[30] However, with exception to this particular unassigned diffraction peak all other peaks up to 20 GPa can be indexed using the ambient phase

monoclinic structure and so, no first-order structural phase transition was detected up to the highest pressure of this study. The diffraction patterns were analyzed by performing Le Bail refinements using the GSAS[31] software. A typical refined high-pressure profile is shown in Fig. 2(b). Example results of the Le Bail refinements together with the results of the theoretical calculations are summarized in Table I where EOS fit parameter values are also listed.

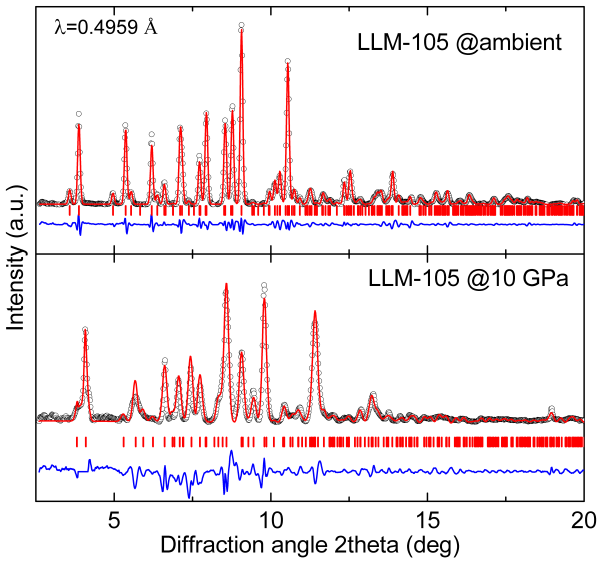

FIG. 2. Le Bail refinements of LLM-105 at (a) ambient pressure and (b) 10 GPa.

From NPT molecular dynamics simulation runs of up to approximately 11 ps we have determined the cell parameters and volume at various pressure conditions and T = 300 K . We allowed an initial equilibration period of 1 ps and discarded this period from our final analysis of the simulations results. In Figure 4, we present example time dependent profiles for results obtained at P=10 GPa. In the figure, the pressure is assumed/computed to be the trace of the stress tensor with the off-diagonal components proving to be very negligible. Figure 4 also has the temperature (T = 300 K), the cell volume, and the lattice parameters temporal profiles. A final set of values at each pressure-temperature run of the cell parameters is obtained by using a block averaging procedure over the complete time period of the simulation, which also yields a standard deviation for the final reported value. A block size of 1 ps was used in the statistical analysis.

The pressure dependent lattice parameters and unit cell volumes for the compression cycle are shown in Figure 5 (a) and (b) respectively together with the results of our ambi-

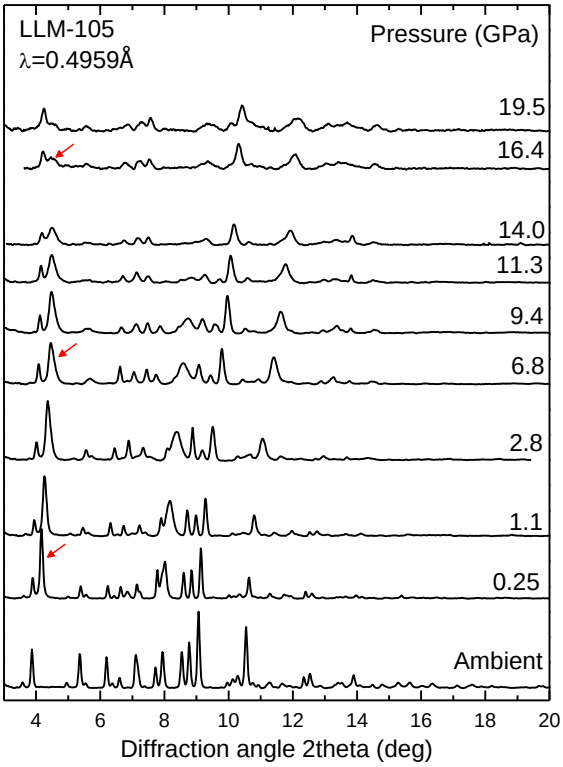

FIG. 3. Selected pressure dependent X-ray diffraction patterns of LLM-105.

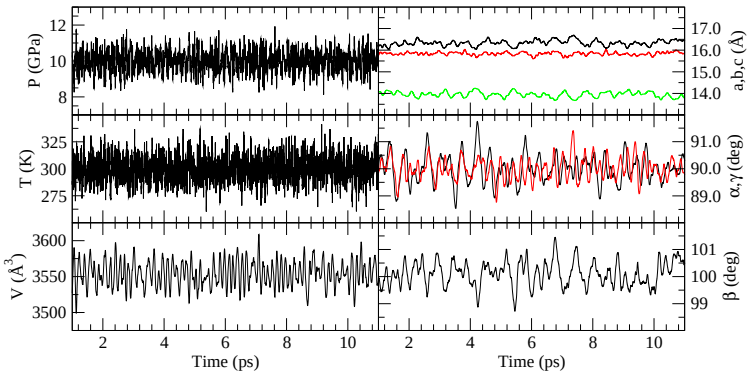

FIG. 4. A sample of computational results of total pressure, temperature, supercell volume and supercell parameters at P = 10 GPa.

ent temperature theoretical calculations. A very good agreement between the two sets of data can be observed from the plots of Fig. 5: (a) *b*-axis as determined in this study is more compressible than a and c axes during initial compression and (b) the theoretically predicted EOS is in agreement with the experimental data. In-line with most high-pressure EOS studies, we conducted unweighted fits of the pressure-volume data using a third-order

Birch−Murnaghan (B-M) equation of state.[32] The corresponding ambient condition bulk modulus *Ko* and the first pressure derivative *K'* results are summarized in Table I.

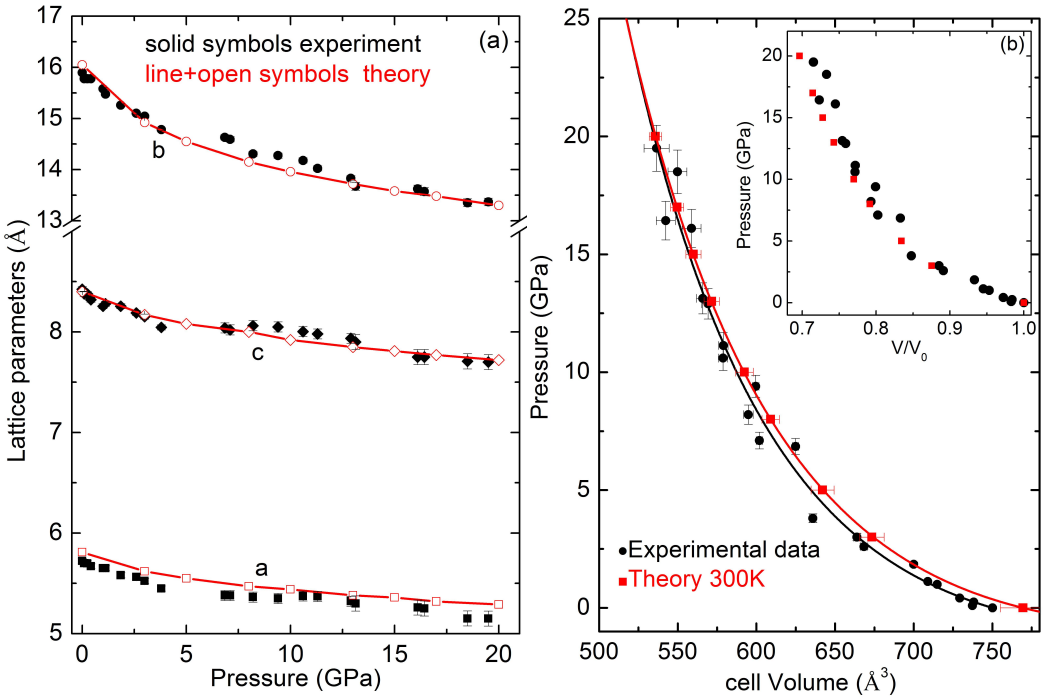

FIG. 5. Pressure dependence of (a) lattice parameters and (b) cell volume V of LLM-105. Experimental results and theoretical predictions with black and red symbols respectively. The solid curves in (b) are the B-M 3rd order EOS fits. The inset in (b) shows the EOS data in relative volume (V/V_0) representation.

To gain deeper insight into how LLM-105 performs under quasi-static compression, we conducted weighted fits and used the reduced χ^2_{red} goodness-of-fit formalism to compare the effectiveness of three EOS models to represent the P-V data. The reduced χ^2_{red} value closest to 1 represents the "winning model". We tested the Birch-Murnaghan,[32] (B-M), 2^{nd} to 5^{th} orders, the Vinet,[33] and the F-f[34] finite strain 1^{st} to 3^{rd} order EOS models. For each winning (best fit) model, where appropriate, we plot corresponding two-dimensional confidence ellipses to reveal two-variable correlation information (see Fig. 6). Bivariable confidence plots enable a more comprehensive basis for comparison of EOS parameters to alternative theoretical and/or experimental results.[35] In this way, one can accurately asses if theoretical results are consistent with experimental results given a range of confidence.

The χ^2_{red} function is used with the assumption that measured values have uncorrelated

TABLE I. Experimental, this study and from Ref. [5], and calculated lattice parameters and cell volumes of LLM-105 at selected pressures. Also listed are the bulk modulus, K_0 and its pressure derivative K' at zero pressure as determined by third-order Birch−Murnaghan (B-M) equation of state unweighted fits.

P(GPa)		a (Å)	b(Å)	c (Å)	Vcell (Å^3)	K (GPa)	K'
0	Expt.	5.723(2)	15.870(2)	8.424(2)	750.08(15)	15(4)	9(3)
0	Expt. (Ref. 5)	5.7159	15.8498	8.4139	748.16		
0	Calc.	5.81(8)	16.05(9)	8.40(5)	769.51(14.36)	12.7(4)	9.4(3)
19.5	Expt.	5.15(8)	13.62(12)	7.74(8)	542(5)		
20	Calc.	5.29(3)	13.3(3)	7.72(2)	535.79(3.92)		

Gaussian distributed error. For the case of a small number (N < 100) of data points, (like most high-pressure EOS studies), the uncertainty of χ^2_{red} values can be unacceptably large; moreover, for nonlinear fitting forms such as higher order EOS models, the "hat"matrix does not exist. In other words, there is no reliable means to compute the number of degrees of freedom, (NDF) for parameters in a nonlinear model; and further, NDFs can vary during an optimization search for a global minimum solution. For these reasons, we also conducted Kolmogorov-Smirnov tests[36,37] (KS-test), *i.e.*, compared converged model fit residuals to a Gaussian distribution with a mean value μ= 0 and a variance of σ^2 =1. The bias (highest region of sensitivity) of a KS-test is selected by the comparative Gaussian mean value distribution value. In some reports, the KS-test has been proven to be more robust than the reduced χ^2_{red} formalism.[38] KS-test values range from 0 (optimal) to 1 (poor). Application of the B-M and Vinet models reveal that the third-order B-M and the Vinet models yielded the statistically best representations of the data. The χ^2_{red} value of the Vinet model is marginally better than the B-M model; and, the Max ΔP values are comparable. The F-f model gives the lowest maximum pressure deviation from the data. The fit results are summarized in Table II. The relatively high χ^2_{red} values from fits to the experimental data indicate that the assessed P-V errors are a bit low given the functional forms of the EOS models. Alternatively, other EOS models may exist that more optimally represent the data where χ^2_{red} values are closer to unity. Fits of the theoretical results, with very low χ^2_{red}

values more clearly indicate that the assessed errors are a bit large (e.g., Vo) given the EOS functional forms.

IV. DISCUSSION

As previously mentioned in the introduction, a series of pressure induced phase transitions have been proposed by a previous theoretical study[14] based on irregular changes of lattice parameters. These results suggest that isostructural phase transitions occur with possibly the same or closely related symmetry. Although no indication of a phase transition can be observed from XRD patterns up to the highest pressure of this study, which rules out a first-order phase transition, we further examine the possibility of a second order isostructutral transition by performing a stress (normalized pressure=F= $P[3f(1 + 2f)^{5/2}]^{-1}$) -Eulerian strain ($f=0.5[(V_0/V)^{2/3}-1]$) (F-f) EOS analysis[39] (Fig. 6). The F-f EOS analysis is ideal to illuminate delicate (low volume discontinuities) structural changes,[40] which are difficult to determine using P-V EOSs.[40,41] Here the Vinet EOS parameters were used as initial guess value inputs for the F-f models. We observe that the pressure dependent stress increases linearly up to the highest achieved pressure, (See Fig. 6(a)). Thus, there is no strong indication of a pressure or strain induced modification to the initial structure. In Figure 6(b) we can also note that our theoretically derived Ko and K' values are not entirely consistent

TABLE II. The most optimal EOS model experimentally and theoretically weighted fits for LLM-105. Note: *K"* is implied for Vinet and F(f) 1^{st} order results (See: O.L. Anderson, 1995 Oxford Univ. Press)

Experimentally Weighted Fits											
B-M order	V_0	V_0 esd	K_0	K_0 esd	K'	K' esd	K"	K" esd	χ^2_{red}	Max ΔP	KS-test
3	750.1005	0.2852	11.8363	1.1623	17.7905	4.5725	[-17.5611]	[11.1751]	14.4669	9.2728	0.6214
Vinet EOS	V_0	V_0 esd	K_0	K_0 esd	K'	K' esd	K"	K" esd	χ^2_{red}	Max ΔP	KS-test
	750.0378	0.3275	13.1417	0.9188	11.9140	1.9647	[-3.1134]	[0.9896]	11.8954	10.3653	0.5648
F-f order	V_0	V_0 esd	K_0	K_0 esd	K'	K' esd	K"	K" esd	χ^2_{red}	Max ΔP	KS-test
1	750.1000	1.0000	15.3196	1.3986	8.9599	1.2075	[-2.1834]	[0.8835]	3.9560	5.2977	0.2576
Theoretically Weighted Fits											
B-M order	V_0	V_0 esd	K_0	K_0 esd	K'	K' esd	K"	K" esd	χ^2_{red}	Max ΔP	KS-test
3.0000	769.5273	0.3025	12.3797	0.1433	9.7180	0.1255	[-3.4171]	[0.1321]	0.0046	0.1169	0.4711
F-f order	V_0	V_0 esd	K_0	K_0 esd	K'	K' esd	K"	K" esd	χ^2_{red}	Max ΔP	KS-test
1.0000	769.5100	14.3600	12.5620	0.1459	9.5479	0.1340	[-3.2014]	[0.1343]	0.0013	0.0972	0.4860

with our experimental results at 99.7 % confidence levels. We believe this inconsistency is primarily due to the theoretical Vo value, which is much higher than the experimental result.

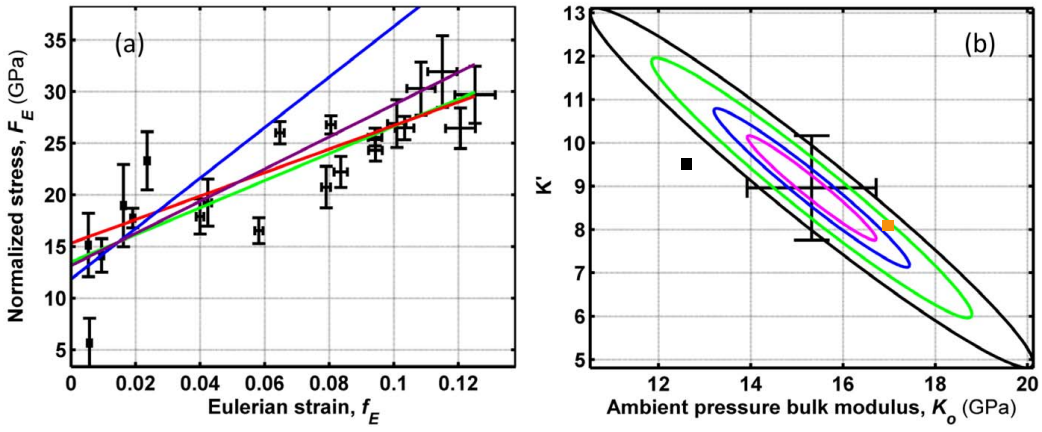

FIG. 6. a) LLM-105 cold-compression data fit to a first-order F-f model. The green line represents an unweighted fit and the red line is an experimentally weighted fit. The blue line is from a 3rd order B-M weighted fit and the violet line is a Vinet EOS mode lweighte fit. b) Plotted confidence ellipses for the F-f fit. The magenta colored ellipse is 0.607-σ (50.3 % confidence), blue is 1-σ (68.3 % confidence), green is 2-σ (95.4% confidence), and the black ellipse is 3-σ (99.7% confidence). The solid black square is the theoretical result and the solid orange square is an experimental result for TATB.

It is interesting to compare the bulk modulus K_0 and its pressure derivative K'_0 of LLM-105 determined in this study with other molecular crystals. Such a comparison can provide valuable information about intermolecular interactions.[42] First, K'_0 appears to be in the same range with large elemental molecules, e.g. S_8 $K'_0 = 8.8$[43] and cyclic organic molecules.[44] TATB, which is an insensitive high explosive cyclic molecule, exhibits K_0 and K'_0 values that place well within the 50 % confidence ellipse of LLM-105.[45] High pressure derivative values e.g., $K' \gg 4$ are usually representative of molecular crystals consisting of large molecules. K'_0 can be expressed as[46] $K'_0=m+n+2$ in the approximation of a simple power potential $U(V)=A/V^m - B/V^n$. Larger molecular size is expected to result in a higher order repulsive term and consequently to a higher K'_0.[42] On the other hand, the bulk modulus of LLM-105 appears to be much larger (almost double in experiment and in theory) in comparison to aforementioned compounds. It is plausible to attribute the higher value of K_0 in the case of LLM-105 and TATB to the presence of extensive hydrogen bonding network, which may

also enhance insensitivity to shock and thermal insults.

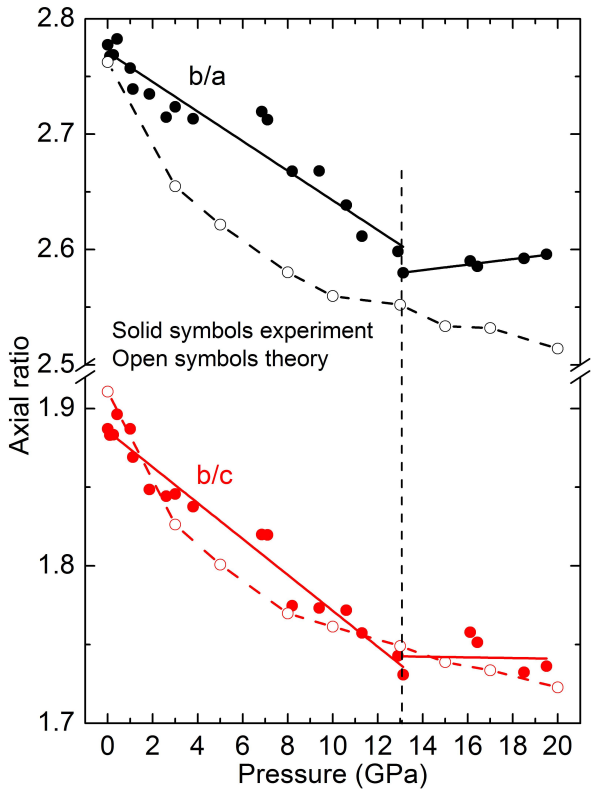

FIG. 7. Pressure dependent axial ratios b/a and b/c of LLM-105. Experimental results and theoretical predictions with black and red symbols respectively. The black solid lines are linear fits of the experimental data below and above 13 GPa, and the dashed red curves are guides to the eye. The vertical dashed line highlights the pressure where the pressure dependence of the axial ratios bcomes pressure invariant.

LLM-105 exhibits higher compressibility along the b-axis as predicted by theoretical studies[13,14] and reported in a previous experimental[8] study. This anisotropic compressibility is attributed to the 2D book-like sheet arrangement[9] of LLM-105 molecules (Fig. 1). Asymmetric expansion of the unit cell upon heating and asymmetric contraction upon compression are consistent with the previously reported book-like sheet structure perpendicular to the b-axis, which results in increased repulsion between neighboring atoms in the a and c directions.[13] This is better highlighted in the plots of the axial ratios of Fig. 7. As can be clearly seen, both b/a and b/c axial ratios decrease linearly up to $\approx$ 13 GPa. Above this pressure both axial ratios become pressure invariant up to 20 GPa. This signals an increase in compressibility along the b-axis, which becomes equal with the other two axes. Inspec-

tion of intermolecular distances reveals that at a critical pressure of 13 GPa the distance between molecules in adjacent sheets is comparable with the intermolecular distance inside the sheets. This in turns affects repulsion between neighboring atoms in b direction and results in measurably lower compressibility. Here the theoretical results are not as definitive with regard to this trend given that both axial ratios continue to decrease above 13 GPa, albeit with smaller slope. It may be that the critical pressure is more pronounced for nonhydrostatic compression. Further, the calculations are conducted on a single crystal of LLM-105, whereas the experimental determinations are derived from polycrystalline powder samples.

V. CONCLUSION

The high-pressure structural behavior of LLM-105 has been explored by a joint experimental and first-principles study up to 20 GPa. As concluded from both the X-ray diffraction measurements and the theoretical calculations, no structural phase transition has been observed up to this pressure. However, a prominent change of the compressibility of b-axis is observed at approximately 13 GPa, which is attributed to the decrease of the distance between molecules in adjacent sheets. At 13 GPa, the inter-sheet distance is comparable with intermolecular distances along individual sheets. The respective bulk moduli and corresponding pressure derivatives were derived from weighted and unweighted fits using selected (relatively optimal) EOS models. The EOS results will improve the confidence of thermochemical modeling predictions of high pressure-temperature detonation reactions of energetic materials including LLM-105.

ACKNOWLEDGMENTS

This work was performed under the auspices of the U. S. Department of Energy by Lawrence Livermore National Security, LLC under Contract DE-AC52-07NA27344. Support from the Computational Grand Challenge Program was instrumental in conducting the computationally intensive atomistic simulations, and is greatly appreciated. The experimental study was supported by the high explosives science campaign II program at Lawrence Livermore National Laboratory. The Advanced Light Source is supported by the Director,

Office of Science, Office of Basic Energy Sciences, of the U.S. Department of Energy under Contract No. DE-AC02-05CH11231. We thank Alastair MacDowell at Lawrence Berkeley National Laboratory for his efforts to facilitate the experiment and Jared C. Gump and Larry E. Fried for helpful discussions and support. B.K. acknowledges financial support from LLNL on subcontract number B608474 and additional support provided by The Scientific and Technological Research Council of Turkey fellowship under Contract No: 114C120.

REFERENCES

[1]E. Stavrou, M. Ahart, M. F. Mahmood, and A. F. Goncharov, Sci. Rep. **3**, (2013).

[2]C. M. Tarver, P. A. Urtiew, and T. D. Tran, J. Energ. Mater. **23**, 183 (2005).

[3]T. D. Tran, P. F. Pagoria, D. M. Hoffman, B. Cunningham, J. L. Cutting, R. S. Lee, and R. L. Simpson, Presented at the 12th International Detonation Symposium, San Diego, CA, August 11-16 (2002).

[4]P. F. Pagoria, A. R. Mitchell, R. D. Schmidt, R. Simpson, F. Garcia, J. W. Forbes, R. Swansiger, and D. Hoffman, "Synthesis, scale-up and characterization of 2,6-diamino-3,5-dinitropyrazine-1-oxide," Tech. Rep. UCRL-JC- 130518 (Lawrence Livermore National Laboratory, 1998).

[5]R. D. Gilardi and R. J. Butcher, Acta Crystallogr. E **57**, o657 (2001).

[6]J. Chen, Z. Qiao, L. Wang, F. Nie, G. Yang, and H. Huang, Mater. Lett. **65**, 1018 (2011).

[7]J. C. Gump, C. A. Stoltz, B. G. Freedman, and S. M. Peiris, Shock Compression of Condensed Matter - 2009, Pts 1 and 2 **1195**, Amer Phys Soc, Topical Grp (2009).

[8]J. C. Gump, C. A. Stoltz, B. P. Mason, B. G. Freedman, J. R. Ball, and S. M. Peiris, J. Appl. Phys. **110**, 073523 (2011).

[9]M. Hai-Xia, S. Ji-Rong, Z. Feng-Qi, G. Hong-Xu, and H. Rong-Zu, Chin. J. Chem. **26**, 1997 (2008).

[10]X. Zhao and Z. Liu, J. Chem. Res. **37**, 425 (2013).

[11]F. Gouranlou and I. Kohsari, Asian J. Chem. **19**, 4309 (2007).

[12]W. D. He, G. Zhou, N. B. Wong, A. M. Tian, and X. P. Long, THEOCHEM **723**, 217 (2005).

[13]M. R. Manaa, I.-F. W. Kuo, and L. E. Fried, J. Chem. Phys. **141**, 064702 (2014).

[14]Q. Wu, C. Yang, Y. Pan, F. Xiang, Z. Liu, W. Zhu, and H. Xiao, J. Mol. Model. **19**, 5159 (2013).

[15]W. Xu, C. An, J. Wang, J. Dong, and X. Geng, Propellants Explos. Pyrotech. **38**, 136 (2013).

[16]B. B. Averkiev, M. Y. Antipin, I. L. Yudin, and A. B. Sheremetev, J. Mol. Struct. **606**, PII S0022 (2002).

[17]M. Matsui, International Conference On High Pressure Science and Technology, Joint AIRAPT-22 and HPCJ-50 **215**, 012197 (2010).

[18]K. Syassen, High Pres. Res. **28**, 75 (2008).

[19]S. Klotz, J.-C. Chervin, P. Munsch, and G. L. Marchand, J. Phys. D: Appl. Phys. **42**, 075413 (2009).

[20]A. P. Hammersley, S. O. Svensson, M. Hanfland, A. N. Fitch, and D. Hausermann, High Pres. Res. **14**, 235 (1996), 4th Workshop of the IUCr High Pressure Group on Synchrotron and Neutron Sources, KEK, JAPAN, MAR 22-24, 1995.

[21]J. P. Perdew, K. Burke, and M. Ernzerhof, Phys. Rev. Lett. **78**, 1396 (1997).

[22]S. Grimme, J. Comput. Chem. **27**, 1787 (2006).

[23]S. Goedecker, M. Teter, and J. Hutter, Phys. Rev. B **54**, 1703 (1996).

[24]J. Schmidt, J. VandeVondele, I. . F. W. Kuo, D. Sebastiani, J. I. Siepmann, J. Hutter, and C. J. Mundy, J. Phys. Chem. B **113**, 11959 (2009).

[25]J. VandeVondele and J. Hutter, J. Chem. Phys. **118**, 4365 (2003).

[26]G. J. Martyna, M. E. Tuckerman, D. J. Tobias, and M. L. Klein, Mol. Phys. **87**, 1117 (1996).

[27]S. Nose, J. Chem. Phys. **81**, 511 (1984).

[28]G. Lippert, J. Hutter, and M. Parrinello, Mol. Phys. **92**, 477 (1997).

[29]J. VandeVondele, M. Krack, F. Mohamed, M. Parrinello, T. Chassaing, and J. Hutter, Comput. Phys. Commun. **167**, 103 (2005).

[30]J. Gump, (2014), private communication.

[31]A. C. Larson and R. B. Von Dreele, "General structure analysis system (GSAS)," Los Alamos National Laboratory Report LAUR 86-748 (2004), available at.

[32]F. Birch, J. Geophys. Res. **83**, 1257 (1978).

[33]P. Vinet, J. Ferrante, J. R. Smith, and J. H. Rose, J. Phys. C **19**, L467 (1986).

[34]F. Birch, Phys. Rev. **71**, 809 (1947).

[35]R. J. Angel, Rev. Mineral Geochem. **41**, 35 (2000).

[36]A. Kolmogov, Giornale dell Istitutano degli Attuari **4**, 83 (1933).

[37]N. Smironov, Annals of Mathematical Statistics **19**, 279 (1944).

[38]G. Andrae, T. Schulze-Hartung, and P. Melchior, "Arxiv e-prints 1012.3754v1," (2010).

[39]D. L. Heinz and R. Jeanloz, J. Appl. Phys. **55**, 885 (1984).

[40]A. Polian, M. Gauthier, S. Souza, D. Trichês, J. a. Cardoso de Lima, and T. Grandi, Phys. Rev. B **83**, 113106 (2011).

[41]B. Godwal, S. Speziale, S. Clark, J. Yan, and R. Jeanloz, J. Phys. Chem. Solids **71**, 1059 (2010).

[42]M. A. Tuktabiev, S. V. Popova, V. V. Brazhkin, A. G. Lyapin, and Y. Katayama, J. Phys.: Condens. Matter **21**, 385401 (2009).

[43]S. Vaidya and G. Kennedy, J. Phys. Chem. Solids **33**, 1377 (1972).

[44]S. Vaidya and G. Kennedy, J. Chem. Phys. **55**, 987 (1971).

[45]L. L. Stevens, N. Velisavljevic, D. E. Hooks, and D. M. Dattelbaum, Propellants Explos. Pyrotech. **33**, 286 (2008).

[46]I. Aleksandrov, A. Goncharov, A. Zisman, and S. Stitshov, Soviet Physics - JETP **66**, 384 (1987).